doi:10.1093/brain/awv086 BRAIN 2015: 138; 1568–1582 | 1568

BRAIN
A JOURNAL OF NEUROLOGY

Evidence for early neurodegeneration in the cervical cord of patients with primary progressive multiple sclerosis

Khaled Abdel-Aziz,[1,2] Torben Schneider,[1,3] Bhavana S. Solanky,[1,3] Marios C. Yiannakas,[1,3] Dan R. Altmann,[1,4] Claudia A. M. Wheeler-Kingshott,[1,3] Amy L. Peters,[5] Brian L. Day,[5] Alan J. Thompson[1,2,6] and Olga Ciccarelli[1,2,6]

Spinal neurodegeneration is an important determinant of disability progression in patients with primary progressive multiple sclerosis. Advanced imaging techniques, such as single-voxel ^{1}H-magnetic resonance spectroscopy and q-space imaging, have increased pathological specificity for neurodegeneration, but are challenging to implement in the spinal cord and have yet to be applied in early primary progressive multiple sclerosis. By combining these imaging techniques with new clinical measures, which reflect spinal cord pathology more closely than conventional clinical tests, we explored the potential for spinal magnetic resonance spectroscopy and q-space imaging to detect early spinal neurodegeneration that may be responsible for clinical disability. Data from 21 patients with primary progressive multiple sclerosis within 6 years of disease onset, and 24 control subjects were analysed. Patients were clinically assessed on grip strength, vibration perception thresholds and postural stability, in addition to the Expanded Disability Status Scale, Nine Hole Peg Test, Timed 25-Foot Walk Test, Multiple Sclerosis Walking Scale-12, and Modified Ashworth Scale. All subjects underwent magnetic resonance spectroscopy and q-space imaging of the cervical cord and conventional brain and spinal magnetic resonance imaging at 3 T. Multivariate analyses and multiple regression models were used to assess the differences in imaging measures between groups and the relationship between magnetic resonance imaging measures and clinical scores, correcting for age, gender, spinal cord cross-sectional area, brain T_2 lesion volume, and brain white matter and grey matter volume fractions. Although patients did not show significant cord atrophy when compared with healthy controls, they had significantly lower total *N*-acetyl-aspartate (mean 4.01 versus 5.31 mmol/l, $P = 0.020$) and glutamate-glutamine (mean 4.65 versus 5.93 mmol/l, $P = 0.043$) than controls. Patients showed an increase in q-space imaging-derived indices of perpendicular diffusivity in both the whole cord and major columns compared with controls ($P < 0.05$ for all indices). Lower total *N*-acetyl-aspartate was associated with higher disability, as assessed by the Expanded Disability Status Scale (coefficient = -0.41, $0.01 < P < 0.05$), Modified Ashworth Scale (coefficient = -3.78, $0.01 < P < 0.05$), vibration perception thresholds (coefficient = -4.37, $P = 0.021$) and postural sway ($P < 0.001$). Lower glutamate-glutamine predicted increased postural sway ($P = 0.017$). Increased perpendicular diffusivity in the whole cord and columns was associated with increased scores on the Modified Ashworth Scale, vibration perception thresholds and postural sway ($P < 0.05$ in all cases). These imaging findings indicate reduced structural integrity of neurons, demyelination, and abnormalities in the glutamatergic pathways in the cervical cord of early primary progressive multiple sclerosis, in the absence of extensive spinal cord atrophy. The observed relationship between imaging measures and disability suggests that early spinal neurodegeneration may underlie clinical impairment, and should be targeted in future clinical trials with neuroprotective agents to prevent the development of progressive disability.

1 NMR Research Unit, UCL Institute of Neurology, London, UK
2 Department of Brain Repair and Rehabilitation, UCL Institute of Neurology, London, UK
3 Department of Neuroinflammation, UCL Institute of Neurology, London, UK
4 Medical Statistics Department, London School of Hygiene and Tropical Medicine, London, UK

Received September 18, 2014. Revised December 11, 2014. Accepted January 27, 2015. Advance Access publication April 11, 2015

5 Sobell Department, UCL Institute of Neurology, London, UK
6 National Institute of Health Research, University College London Hospitals, Biomedical Research Centre, London, UK

Correspondence to: Khaled Abdel-Aziz,
NMR Research Unit,
Queen Square Multiple Sclerosis Centre,
Department of Brain Repair and Rehabilitation,
UCL Institute of Neurology,
Queen Square House,
Queen Square, London,
WC1N 3BG,
UK
E-mail: k.abdel-aziz@ucl.ac.uk

Keywords: multiple sclerosis imaging; biomarkers; cellular mechanisms

Abbreviations: ADC = apparent diffusion coefficient; FWHM = full-width half-maximum; Glx = glutamate-glutamine; ^{1}H-MRS = ^{1}H-magnetic resonance spectroscopy; PPMS = primary progressive multiple sclerosis; P0 = zero displacement probability; QSI = q-space imaging; tNAA = total *N*-acetyl-aspartate

Introduction

The clinical phenotype of primary progressive multiple sclerosis (PPMS) is characterized by sustained disability progression from disease onset and is typically associated with severe locomotor disability (Thompson *et al.*, 2000), with a median time to Disability Status Scale 6 (walking with a cane) of between 6 and 8.5 years (Runmarker and Andersen, 1993; Cottrell *et al.*, 1999; Confavreux *et al.*, 2000). The rate of disability progression is highly variable, but occurs more quickly early in the disease course and reflects, in part, neuroaxonal loss and neuronal dysfunction in the spinal cord (Bjartmar *et al.*, 2000). There would be great value in developing and applying imaging markers of neurodegenerative processes to the spinal cord in early PPMS in order to improve our understanding of the early pathological events that occur in the injury pathway responsible for clinical disability. This step is considered to be crucial in the translational pathway that aims to validate biomarkers that predict clinical outcomes and treatment response in clinical trials (Fox *et al.*, 2012).

Advanced quantitative MRI has been applied in the brain in early PPMS and has improved our understanding of the mechanisms leading to tissue damage, beyond that associated with macroscopic T_2 lesions (Wheeler-Kingshott *et al.*, 2014). Measures provided by diffusion tensor imaging and ^{1}H-magnetic resonance spectroscopy (^{1}H-MRS), have been shown to correlate with disability (Sastre-Garriga *et al.*, 2005; Ramio-Torrenta *et al.*, 2006; Bodini *et al.*, 2013) and predict progression (Khaleeli *et al.*, 2007, 2008). Applying similar techniques to the spinal cord has been technically challenging (Wheeler-Kingshott *et al.*, 2014). However, recent developments have led to applications of advanced quantitative MRI in the spinal cord in relapsing-remitting multiple sclerosis and have provided insights into underlying spinal tissue pathology (Ciccarelli *et al.*, 2007, 2013; Farrell *et al.*, 2008; Marliani *et al.*, 2010; Kearney *et al.*, 2014).

One of the most promising quantitative MRI techniques is high b-value q-space imaging (QSI), a model-free diffusion weighted imaging technique (Callaghan *et al.*, 1988). QSI is thought to be highly specific for axonal injury (Assaf *et al.*, 2005) and has shown better sensitivity for detecting pathophysiological changes within lesions and normal-appearing white matter, compared to diffusion tensor imaging in the brains of patients with multiple sclerosis (Assaf *et al.*, 2002). A small pilot study in relapse-onset multiple sclerosis demonstrated the feasibility of using high b-value QSI in the spinal cord with improved detection of abnormal diffusion compared with the conventional diffusion weighted image acquisition and analysis (Farrell *et al.*, 2008).

Spinal cord ^{1}H-MRS is used to quantify metabolites that reflect specific pathological processes and can complement structural imaging (Ciccarelli *et al.*, 2014). Commonly quantified metabolites in the spinal cord include: total *N*-acetyl-aspartate (tNAA), a marker of neuroaxonal integrity and metabolic function (Moffett *et al.*, 2007), myo-inositol, a marker of astrocytic activation and proliferation (Brand *et al.*, 1993) and total choline, which reflects changes in steady-state levels of membrane phospholipids released during myelin breakdown (Henning *et al.*, 2008; Marliani *et al.*, 2010). More recently, our group developed a new protocol capable of quantifying glutamate-glutamine (Glx), a marker of neuronal integrity and neurotransmitter pool, in the spinal cord (Solanky *et al.*, 2013). Although there have been a few studies of the spinal cord using MRS in patients with relapsing-remitting multiple sclerosis and neuromyelitis optica, which have consistently shown neuronal loss and metabolic dysfunction, as reflected by reduced concentration in tNAA in the cervical cord of patients compared to controls (Ciccarelli *et al.*, 2007, 2013; Marliani *et al.*, 2007), to date none have included patients with PPMS.

Besides the need to utilize more pathologically specific *in vivo* spinal cord imaging techniques, there is also a need to incorporate objective clinical measures, which are more sensitive to changes in clinical functions mediated by spinal pathways than conventional clinical tests, such as the Expanded Disability Severity Scale (Kurtzke, 1983). Measures such as postural stability, vibration perception thresholds and dynamometry are more responsive to small clinical changes due to damage in the spinal cord than the Expanded Disability Status Scale, and have been shown to increase the sensitivity for detecting correlations between MRI abnormalities in the spinal cord and disability (Zackowski *et al.*, 2009; Oh *et al.*, 2013).

In the current study we used a combination of MRS and QSI to investigate changes in the cervical cord, which underlie disability in patients with early PPMS, to test two hypotheses: (i) MRS and QSI demonstrate early neurodegeneration in the upper cervical cord in patients with PPMS before the occurrence of spinal cord atrophy; and (ii) in patients, there is a relationship between MRS and QSI measures and disability, as reflected by newer spinal cord-specific clinical scores, alongside standard multiple sclerosis clinical scales, suggesting that early spinal cord neurodegeneration is linked with clinical impairment in PPMS.

Materials and methods

Study participants

We prospectively recruited patients with a diagnosis of PPMS (Polman *et al.*, 2005) aged 18–65 years, within 6 years from disease onset, as well as age and gender-matched control subjects. On the day of the MRI, patients were clinically assessed. All subjects provided written, informed consent prior to taking part in the study, which was approved by our local research ethics committee.

Clinical assessments

All patients were assessed using conventional clinical scales, including the Expanded Disability Status Scale (Kurtzke, 1983), Nine Hole Peg Test (Goodkin *et al.*, 1988) and Timed 25 Foot Walk Test (Cutter *et al.*, 1999). For the purpose of statistical analysis, the average of two trials of the Timed Walk Test and the average of four trials of the Nine Hole Peg Test (averaged as reciprocals of the mean times from two trials for each hand) (Fischer *et al.*, 1999) were calculated. We also used the Multiple Sclerosis Walking Scale-12 (Hobart *et al.*, 2003), and the Modified Ashworth Scale (Bohannon and Smith, 1987). The Modified Ashworth Scale values from 16 muscle groups in the upper and lower limbs were converted from a 0–4 scale (which includes a value of 1+ between scores of 1 and 2) to a 0–5 scale; the resulting values were summated to obtain an overall score ranging from 0 to 80 (Stein *et al.*, 2007).

Clinical scales with the potential to be sensitive to spinal cord pathways injury were also applied, including the mean grip strength from both upper limbs using the Jamar hydraulic dynamometer (Sammons Preston Inc.) (Svens and Lee, 2005), and the vibration perception thresholds, which were measured from all four limbs at the lateral malleoli and ulna styloid processes, using the biosthesiometer (Bio-Medical Instrument Co.). Mean vibration perception thresholds were calculated and used in the analysis. Finally, postural stability was assessed using a modified version of a recently described protocol for quantifying stance instability (Bunn *et al.*, 2013). Subjects were asked to stand relaxed and still, facing a blank wall at a distance of 1 m, in a well-lit room, for 40 s trials. Three trials under each of the four conditions were recorded, consisting of two stance widths (inter-malleolar distance of 32 cm and 4 cm) under two visual conditions (eyes either open or closed). Body sway was measured using a 3D orientation sensor (MTx: Xsens), which was fixed to the skin, just below the C7 spinous process. The device measured the instantaneous angular position of the trunk in the anteroposterior (pitch) and mediolateral (roll) planes and was sampled at 100 Hz. Summary measures were made on these signals using custom scripts written in Matlab (The Mathworks). The raw data were low-pass filtered at 10 Hz using a zero-phase, 5th order Butterworth filter. The amount of angular motion was then calculated separately for the roll and pitch body sway data and from the combined motion given by square root (pitch-motion^2 + roll-motion^2), termed total sway. All three signals were summarized by summing the sample-to-sample absolute change in signal and then dividing by the duration of the trial to yield average angular speeds of body sway reported in °/s. The mean of the three trials per condition were used for statistical analysis. An index of exacerbation of sway on eye closure was obtained from the Romberg quotient calculated as sway eyes closed/sway eyes open at both stance widths.

Spinal cord and brain MRI protocol

All scans were performed using a 3 T Achieva system (Philips Medical Systems). To reduce motion artefacts during scanning and improve image quality, a magnetic resonance compatible cervical collar was worn by all volunteers (Yiannakas *et al.*, 2012).

Using the manufacturer's 16-channel neurovascular coil (Phillips Healthcare Systems), single voxel MRS was performed using a recently optimized protocol (Solanky *et al.*, 2013). Conventional turbo spin-echo sequences were used to acquire structural images for radiological reading and to guide voxel placement. T_2-weighted images were acquired in the coronal plane (parameters: repetition time = 4000 ms; echo time = 100 ms; field of view = 160 × 250 mm^2; voxel size = 0.6 × 0.6 × 3.0 mm^3; number of excitations = 2; 13 contiguous slices; scan time = 1:36 min) and proton density/T_2-weighted images were acquired in the sagittal plane using a dual echo turbo spin-echo sequences (parameters: repetition time = 4000 ms; echo time = 15/80 ms; field of view = 256 × 160 mm^2; echo train length = 12; voxel size = 1.0 × 1.0 × 3.0 mm^3; number of excitations = 2; 12 contiguous slices; scan time = 5:44 min). For spectroscopy, volumes of interest with dimensions of ~5.4 × 7.76 × 55 mm^3 (2.3 ml) were prescribed using the reference images and centred on the C2–3 intervertebral disc (Fig. 1). The dimensions of the volumes of interest were adjusted in the anterior-posterior direction dependent on the size of each volunteer's spinal cord

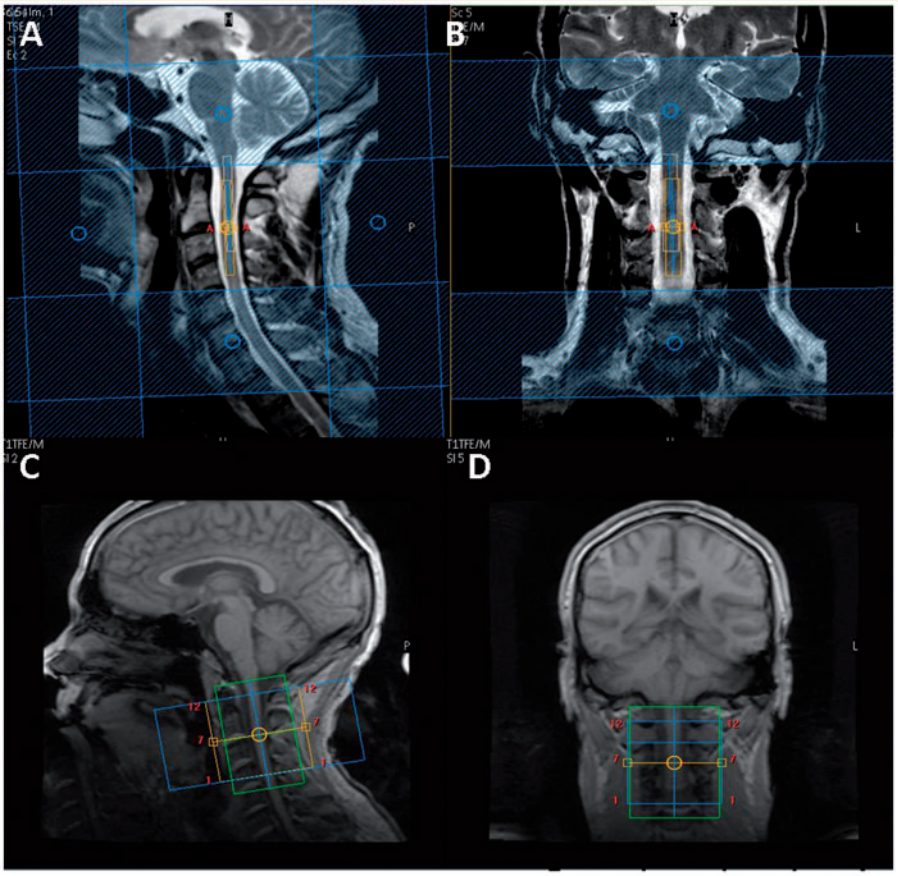

Figure 1 Planning of spectroscopy voxel and diffusion weighted image volume. Sagittal (**A**) and coronal (**B**) T_2-weighted images of the cervical cord with spectroscopy voxel centred on C2–3 intervertebral disc. Sagittal (**C**) and coronal (**D**) T_1-weighted image of the cervical cord showing diffusion weighted imaging volume coverage centred on the C2–3 disc.

(Ciccarelli *et al.*, 2007; Marliani *et al.*, 2010). MRS data were acquired using a point resolved spectroscopy (PRESS) localization sequence [parameters: echo time = 30 ms; 376 averages with triggered, first order iterative shimming, multiply optimized insensitive suppression train (MOIST) water suppression, four outer volume suppression slabs in the anterior-posterior direction and rostrocaudal directions and cardiac gating (repetition time = 3RR $\approx$ 3000 ms) using a peripheral pulse unit (350 ms delay), scan time = 19:42 min].

For cord mean cross-sectional area measurements and confirmation of lesion location, the cervical cord was imaged in the axial plane, perpendicular to the longitudinal axis of the cord with the imaging volume centred on the C2–3 intervertebral disc, using a fat-suppressed 3D slab-selective fast field echo sequence (parameters: repetition time = 23 ms; echo time = 5 ms; flip angle $\alpha = 7°$; field of view = $240 \times 180\,mm^2$; voxel size = $0.5 \times 0.5 \times 5\,mm^3$; number of excitations = 8; 11 axial contiguous slices; scan time = 15:58 min). In order to match the position and orientation of the volumetric scan to the spectroscopy voxel, the prescription values used for the MRS acquisition were copied and manually entered by the operator when setting up the 3D fast field echo scan.

Using the manufacturer's 32-channel head coil (Philips Medical Systems), each subject underwent a cardiac gated diffusion weighted imaging acquisition [parameters: voxel size = $1 \times 1 \times 5\,mm^3$ (interpolated in *k*-space to a $0.5 \times 0.5\,mm^2$ in-plane resolution) field of view = $64 \times 64\,mm^2$; repetition time = 9RR, echo time = 129 ms] performed with the volume centred on the C2–3 disc to ensure similar coverage as the spectroscopy voxel; 12 axial contiguous slices covering a 60 mm length of the cervical cord, typically giving coverage of the C1–3 spinal segments (Fig. 1). The 32-channel head coil was used because it gave superior signal-to-noise ratio during QSI sequence optimization experiments (Schneider *et al.*, 2011). A ZOOM sequence was used with outer-volume suppression to minimize artefacts (Wilm *et al.*, 2007). Thirty diffusion weighted image volumes with equally spaced q-values (Farrell *et al.*, 2008) and two non-diffusion weighted (b0) volumes were acquired with diffusion weighting in two perpendicular (x and y) directions and one parallel (z) direction relative to the main axis of the spinal cord (parameters: diffusion pulse duration $\delta = 11.4$ ms, diffusion time $\Delta = 75$ ms, gradient strength G linearly increased in 31 steps from 0 to 87.5 mT/m in x and y direction and 62 mT/m in z direction; scan time = 22:28 min).

To achieve the maximum possible gradient strength on the scanner, we exploited the combination of parallel gradient amplifiers in the scanner, which each generate a maximum diffusion gradient strength of 62 mT/m along the major axis of the scanner bore. Assuming axial symmetry of the axons along the long axis of the spinal cord, we applied gradient amplifiers in two orthogonal directions that maximize gradient

strength perpendicular to axis of the spinal cord (Supplementary Fig. 1). This allowed us to generate a guaranteed maximum gradient strength of $\sqrt{2}*62$ mT/m in the *xy* direction. In the *z* direction we use a maximum gradient of 62 mT/m. Q-values were the same in the *xy* and *z* directions, but the increase in gradient strength allowed us to use a smaller gradient pulse duration of 11.4 ms in the *xy* direction (16 ms in *z*). The full protocol is given in Supplementary Table 1.

For the calculation of brain T_2 lesion volumes, proton density/T_2-weighted images were acquired using a dual-echo turbo spin-echo sequence (parameters: repetition time = 3500 ms; echo time = 15/85 ms; flip angle $\alpha = 90°$; field of view = 240 × 180 mm^2; voxel size = 1 × 1 × 3 mm^3; number of excitations = 1; 50 axial contiguous slices; scan time = 4:01 min). For calculation of brain tissue volumes a 3D T_1-weighted magnetization-prepared gradient-echo sequence was used (repetition time = 6.9 ms; echo time = 3.1 ms; inversion time = 824 ms; flip angle $\alpha = 8°$; field of view = 256 × 256 mm^2; voxel size = 1 × 1 × 1 mm^3; number of excitations = 1; 180 sagittal contiguous slices; scan time = 6:31 min).

Imaging post-processing

Spinal cord metabolite quantification

Metabolite concentrations were quantified using the user-independent LCModel (version 6.3) package (Provencher, 1993) and a set of basis spectra, comprising 17 metabolites including the macromolecules, simulated using GAMMA (Smith *et al.*, 1994) as previously described (Solanky *et al.*, 2013). NAA (*N*-acetyl-aspartate) + NAAG (*N*-acetylaspartyl glutamate), (hereafter tNAA), total choline (choline + phosphocholine), total creatine (creatine + phosphocreatine), myo-inositol and Glx concentrations were quantified using the unsuppressed water signal obtained from the same voxel as a reference (Gasparovic *et al.*, 2006) and formed the focus of our analysis. Corrections for T_2 values were not performed because the echo time used is relatively short, compared to the T_2 relaxation times of the metabolites under study (Wansapura *et al.*, 1999; Edden *et al.*, 2007) and, therefore, it is expected that changes in T_2 would be negligible. Measuring T_2 values for each metabolite would not have been possible in a patient cohort within clinically feasible scan times

The signal-to-noise ratio and full-width of half-maximum (FWHM) of the tNAA peak provided by LCModel were used to assess spectral quality and Cramér–Rao Lower Bounds values < 20% for tNAA, total creatine, total choline and myo-inositol and < 30% for Glx were used to confirm the reliability of the spectral fit (Provencher, 2014). Poor quality spectra were excluded from the analysis. Criteria for exclusion were poor water suppression or FWHM of > 0.13 with signal-to-noise ratio of < 3.

Spinal cord cross sectional area measurement

Image segmentation and cross-sectional area measurements were performed using the 3D fast field echo data set in Jim 6.0 Software (Xinapse Systems). Three contiguous 5 mm axial slices, centred on the C2–3 disc were segmented using the active surface model method (Horsfield *et al.*, 2010). The mean cross-sectional area of these three slices was then calculated.

Spinal cord q-space imaging and region of interest analysis

QSI indices from the q-space analysis, which characterize the diffusion properties of water, are derived from the displacement probability density function, which is the average probability of a spin moving a certain distance during a given diffusion time. At a given diffusion time, a tall, narrow displacement probability density function suggests a low diffusion constant and/or restricted diffusion, whereas a low, broad displacement probability density function suggests a high diffusion constant and/or more unrestricted diffusion (Farrell *et al.*, 2008).

The two perpendicular diffusion directions were averaged (*xy*) to increase the signal-to-noise ratio. The measurements were then linearly re-gridded to be equidistant in q-space and the diffusion displacement probability density function was computed using inverse Fast Fourier Transformation. To increase the resolution of the displacement probability density function, the signal was extrapolated in q-space to a maximum q = 200 mm^{-1} by fitting a bi-exponential decay curve to the diffusion weighted imaging data (Farrell *et al.*, 2008). Supplementary Fig. 2 illustrates the processing pipeline.

Data were corrected for motion using 'reg_aladin' from the NiftyReg toolkit (Ourselin *et al.*, 2000). Registration was performed between the interleaved b = 0 acquisitions of the *xy* and *z* protocol using the first b = 0 of the *xy* protocol as reference. The estimated registration was then applied to the intermediate diffusion weighted images. The quality of the motion correction was assessed in each subject and misregistered slices/subjects were excluded from the study.

Voxel-wise maps of the FWHM, which represents the width of the displacement probability density function, and the zero displacement probability (P0), representing the height of the displacement probability density function, were computed for *xy* and *z*. Conventional apparent diffusion coefficient (ADC) maps were also derived from the low b-value part of the decay curve (b < 1100 s/mm^2) for both *xy* and *z* directions, using a constrained non-linear least squares fitting algorithm (Farrell *et al.*, 2008).

To assess region-specific differences in QSI indices, the whole 60 mm length of upper cervical spinal cord was first extracted from CSF and other tissue types, and four regions of interest were created using the appropriate tool in JIM 6.0 and positioned using the b0 images for each axial slice for orientation. ADC and QSI indices were measured from regions of interest in the anterior, right lateral, left lateral and posterior columns, as well as whole cord (Supplementary Fig. 3). No statistical differences were found between QSI indices from the right and left lateral columns; therefore for ease of analysis, a mean value from both columns was calculated for each of the QSI indices.

Brain T_2 lesion volumes and grey matter and white matter volume fractions

Brain T_2-lesion volume was calculated by outlining lesions on T_2-weighted MRI scans using a semi-automated edge finding tool (JIM v. 6.0) by a single observer (K.A.). Total lesion volume was recorded (in ml) for each subject.

To avoid segmentation errors due to white matter lesions, an automated lesion-filling technique was used (Chard *et al.*, 2010). Lesion masks were created based on 3D T_1-weighted

sequences. The lesion-filled images were segmented into white matter, grey matter and CSF, using the 'new segment' option in SPM8 (statistical parametric mapping; Wellcome Trust Centre for Neuroimaging, University College London Institute of Neurology, London). Segmentations were reviewed to exclude errors. White and grey matter fractional volumes, relative to total intracranial volume (the sum of grey matter, white matter and CSF volumes), were calculated.

Statistical analyses

Analyses were performed in Stata 13.1 (Stata Corp.). Adjusted differences between patients and controls were obtained by multiple regression of the relevant imaging measure on a subject type indicator, with age, gender and cross-sectional area as covariates. This analysis was then repeated to evaluate the adjusted difference between controls and patients with and without spinal cord lesions within the C1–3 region of interest. In the case of cross-sectional area, group differences were obtained with a multiple regression model co-varying for age and gender.

In patients, univariable associations between metabolites and whole cord QSI metrics were examined with Pearson correlations. Associations between spinal cord imaging measures and Expanded Disability Status Scale, Modified Ashworth Scale, Nine Hole Peg Test and vibration perception thresholds were examined with multiple regression of the clinical variable on the spinal cord imaging measure as predictor, with the following potential confounders as covariates: age, gender, mean cord area, brain T_2 lesion volume, grey matter fractional volume and white matter fractional volume; because of the large number of covariates, these were entered singly into the model, and the unadjusted association is only reported where it was not materially affected by entering any of these covariates. Where regression residuals showed signs of non-normality (e.g. for Expanded Disability Status Scale), the non-parametric bias corrected and accelerated bootstrap was used (1000–5000 replicates, depending on the *P*-value resolution required), and then, if more precise determination was too computer intensive, the *P*-value was reported as a range.

For associations between spinal cord measures and measures of postural stability, multivariate regression was used because of the highly related nature of the clinical measures: by performing joint tests of association, the danger of spurious significant results was minimized by reporting associations only where the joint test was significant; where the joint test is not significant, there is no global evidence for any of the individual associations tested, in which case these are not reported as significant even when individually $P < 0.05$. The multivariate associations were carried out with potential confounders entered as described above.

Results

Participant demographics and characteristics

Twenty-three patients with early PPMS and 26 healthy controls were recruited. One patient was unable to tolerate the scan and was therefore excluded; a second patient's scans were excluded from the final analysis due to severe motion-related image degradation. Two control subjects were also excluded from the study due to the detection of unexpected pathology on structural spinal cord imaging. Therefore data from 21 patients and 24 age and gender-matched healthy controls were included in the final analysis (Table 1). Patients had short disease duration and mild to

Table 1 Demographic, clinical and radiological characteristics of patients and volunteers

	Healthy controls (*n* = 24)	Patients with PPMS (*n* = 21)
Mean age (SD)	42.1 (11.5) years	48 (7.9) years
Gender	19 F: 5 M	12 F: 9 M
Mean cross-sectional area (SD)	81.8 (8.1) mm^2	77.5 (9.6) mm^2
Mean grey matter volume fraction (SD)	0.48 (0.01)	0.47 (0.01)
Mean white matter volume fraction (SD)	0.34 (0.01)	0.33 (0.01)
Mean brain parenchymal fraction (SD)	0.82 (0.02)	0.80 (0.02)
Mean T_2 lesion volume (SD)		11.6 (9.4) ml
Mean disease duration (SD)		3.9 (1.5) years
Median Expanded Disability Status Scale (range)		5.0 (3.0–6.5)
Mean 25 Foot Timed Walk Test (SD)		8.1 (5.9) s
Mean Multiple Sclerosis Walking Scale-12 (SD)		44.4 (11.4)
Mean summated Modified Ashworth Score (SD)		7.2 (9.3)
Mean Nine Hole Peg Test (SD)		30.0 (13.3) s
Mean grip strength (SD)		50.2 (26.4) lbs force
Mean Vibration Perception Threshold (SD)		10.7 (10.6)
Mean sway, 32 cm, eyes open (SD)		0.87 (0.37) °/s
Mean sway, 32 cm, eyes closed (SD)		1.07 (0.46) °/s
Mean sway, 4 cm, eyes open(SD)		0.98 (0.38) °/s
Mean sway, 4 cm, eyes closed (SD)		1.28 (0.58) °/s

F = female; M = male.

moderate levels of disability; further details on patient characteristics, disability and conventional brain MRI are summarized in Table 1. Conventional MRI of the cervical cord identified cervical cord lesions in 18 of 21 patients (Supplementary Table 2). Of the 18 patients with cervical cord lesions, 12 patients had lesions within the C1 to C3 segments covered by the MRS and QSI volumes.

Spectroscopy quality indicators

Typical post-processed spectra are shown in Fig. 2. The FWHM and signal-to-noise ratio estimated by LCModel (reported as mean ± SD) were 0.11 ± 0.03 ppm and 4.4 ± 1.4, respectively. Mean Cramér–Rao Lower Bounds for each metabolites were: tNAA (8%), total creatine (11%), total choline (10%), myo-inositol (10%) and Glx (21%). The reproducibility of MRS measurements achieved with this protocol have previously been reported (Solanky *et al.*, 2013).

Differences in spinal cord measures between patients and controls

There was no significant difference in cross-sectional area between patients and controls after adjusting for age and gender ($P = 0.092$). Patients had lower spinal tNAA and Glx concentrations than healthy controls after correction for age, gender and cross-sectional area, and this was most marked in patients with spinal cord lesions within the spectroscopic volume (Table 2 and Fig. 2). Myo-inositol concentrations were borderline significantly higher in patients than healthy controls but were significantly elevated in patients with a C1–C3 lesion (Table 2).

Patients had significantly higher perpendicular diffusivity (indicating increased movement of water perpendicular to the main cord axis, as reflected by increased ADC*xy* and FWHM*xy* and reduced P0*xy*), in the whole cord and the anterior, posterior and lateral columns, and a significant increase in parallel diffusivity (ADC*z*) confined to the posterior columns when compared with controls, after adjusting for age, gender and cross-sectional area (Tables 2 and 3 and Fig. 2). Perpendicular diffusivity derived from QSI indices (FWHM*xy* and P0*xy*), but not ADC*xy* was also significantly higher in patients with normal-appearing spinal tissue compared with healthy controls (Table 2).

Univariable analysis of spinal cord metabolite concentrations and q-space imaging metrics in patients

In patients, spinal cord tNAA concentration was negatively correlated with whole cord ADC*xy* ($r = -0.581$, $P = 0.011$) and FWHM*xy* ($r = -0.636$, $P = 0.005$) and positively correlated with whole cord P0*xy* ($r = 0.646$, $P = 0.004$) (Supplementary Fig. 4). Other spinal metabolite concentrations did not correlate significantly with each other, or with cord QSI indices.

Associations between whole cord imaging measures and clinical disability

In patients, following adjustment for age, gender, cross-sectional area, brain T_2 lesion volume, grey matter fractional volume and white matter fractional volume, a

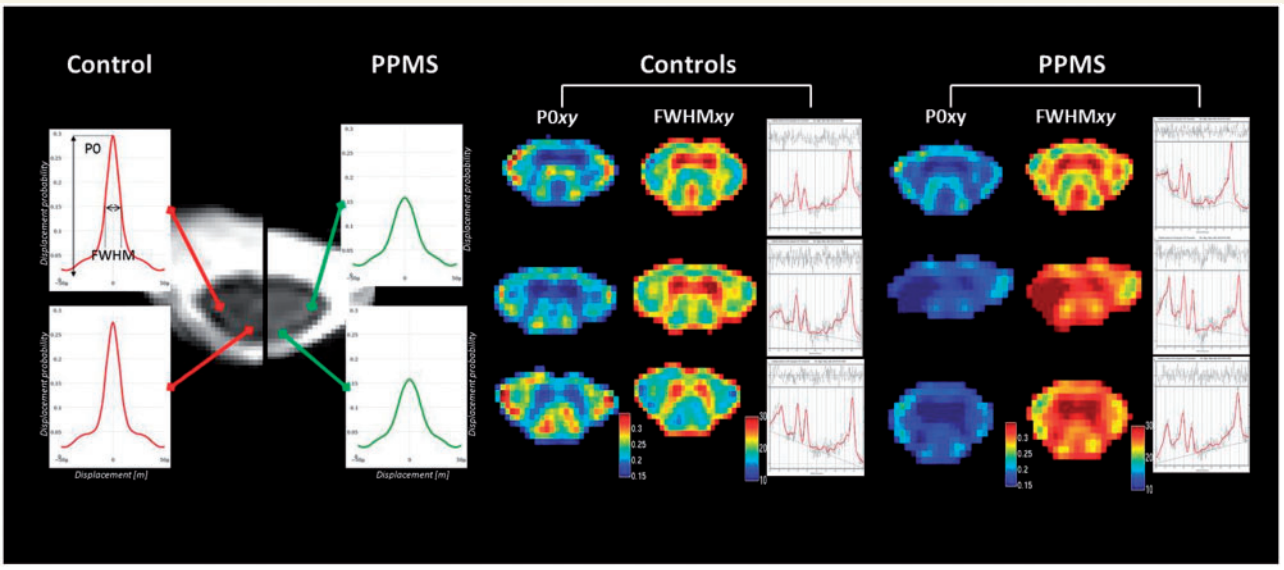

Figure 2 Differences in spinal metabolite concentrations and perpendicular diffusivity between patients and controls. Differences in height and width of the displacement probability density function from the posterior and lateral columns between a healthy control and patient are shown on the *far left*. Grouped P0*xy* maps, FWHM*xy* maps and post-processed spectra from three controls (*centre*) and three patients (*far right*) demonstrate lower probability of zero net displacement (P0*xy*) and increased diffusion distribution (FWHM*xy*) in the patients. The spectra show reduced tNAA and Glx levels in the patients compared to the controls.

Table 2 Summary of mean (SD) metabolite concentrations and QSI indices from the cervical cord of patients and controls and *P*-values for adjusted group comparisons after correcting for age, gender and mean cord cross-sectional area

Spinal cord measure	Healthy controls (*n* = 24)	Patients without C1–3 lesion (*n* = 9)	Patients with C1–3 lesion (*n* = 12)	All patients (*n* = 21)
tNAA (mmol/l)	5.31 (1.47)	4.23 (0.86) *P* = 0.206	3.89 (1.31) *P* = 0.102	**4.01 (1.16)** ***P* = 0.020**
tCho (mmol/l)	1.31 (0.41)	1.12 (0.22) *P* = 0.241	1.33 (0.38) *P* = 0.852	1.26 (0.34) *P* = 0.610
tCr (mmol/l)	3.76 (1.13)	3.04 (0.35) *P* = 0.099	4.22 (1.73) *P* = 0.908	3.79 (1.48) *P* = 0.963
Myo-inositol (mmol/l)	4.49 (1.23)	4.25 (1.17) *P* = 0.287	**6.26 (1.84)** ***P* = 0.006**	5.55 (1.88) *P* = 0.081
Glx (mmol/l)	5.93 (1.66)	5.01 (1.90) *P* = 0.170	**4.50 (0.71)** ***P* = 0.047**	**4.65 (1.11)** ***P* = 0.043**
ADCxy (μm^2/ms)	0.390 (0.09)	0.421 (0.05) *P* = 0.151	**0.481 (0.10)** ***P* = 0.002**	0.454 (0.08) *P* = 0.006
ADCz (μm^2/ms)	1.783 (0.10)	0.183 (0.01) *P* = 0.123	0.183 (0.02) *P* = 0.119	1.834 (0.14) *P* = 0.123
FWHMxy ($\mu m \times 10^2$)	0.236 (0.02)	**0.251 (0.01)** ***P* = 0.020**	**0.276 (0.04)** ***P* < 0.001**	**0.265 (0.03)** ***P* = 0.001**
FWHMz ($\mu m \times 10^2$)	0.550 (0.03)	0.553 (0.03) *P* = 0.427	**0.560 (0.03)** **0.019**	0.557 (0.03) *P* = 0.120
P0xy (a.u)	0.202 (0.02)	**0.188 (0.01)** ***P* = 0.025**	**0.174 (0.03)** **0.001**	**0.180 (0.02)** ***P* = 0.001**
P0z (a.u)	0.113 (0.004)	0.112 (0.003) *P* = 0.278	0.113 (0.004) *P* = 0.481	0.113 (0.004) *P* = 0.470

P-values obtained using a linear regression analysis, correcting for age, gender and cord surface area.
tCho = choline containing compounds; tCr = creatine + phosphocreatine.

Table 3 Summary of mean (SD) QSI indices and ADCs from the major white matter columns of patients and controls

Region of interest	Diffusion measure	Patients with PPMS (*n* = 21)	Healthy controls (*n* = 24)	*P*-value
Anterior column	ADCxy (μm^2/ms)	0.497 (0.15)	0.388 (0.12)	**0.028**
	ADCz (μm^2/ms)	1.921 (0.20)	1.867 (0.17)	0.331
	FWHMxy ($\mu m \times 10^2$)	0.266 (0.04)	0.229 (0.02)	**0.001**
	FWHMz ($\mu m \times 10^2$)	0.562 (0.03)	0.600 (0.04)	0.159
	P0xy (a.u)	0.180 (0.03)	0.210 (0.02)	**0.002**
	P0z (a.u)	0.111 (0.004)	0.111 (0.01)	0.411
Posterior column	ADCxy (μm^2/ms)	0.458 (0.16)	0.368 (0.10)	**0.017**
	ADCz (μm^2/ms)	2.181 (0.26)	2.092 (0.14)	**0.050**
	FWHMxy ($\mu m \times 10^2$)	0.261 (0.06)	0.229 (0.03)	**0.029**
	FWHMz ($\mu m \times 10^2$)	0.610 (0.04)	0.602 (0.04)	0.122
	P0xy (a.u)	0.185 (0.03)	0.208 (0.03)	**0.018**
	P0z (a.u)	0.102 (0.004)	0.103 (0.004)	**0.045**
Mean lateral columns	ADCxy (μm^2/ms)	0.416 (0.11)	0.319 (0.10)	**0.001**
	ADCz (μm^2/ms)	1.989 (0.26)	1.979 (0.12)	0.581
	FWHMxy ($\mu m \times 10^2$)	0.254 (0.04)	0.214 (0.02)	**<0.001**
	FWHMz ($\mu m \times 10^2$)	0.579 (0.02)	0.579 (0.03)	0.318
	P0xy (a.u)	0.189 (0.03)	0.224 (0.03)	**<0.001**
	P0z (a.u)	0.108 (0.007)	0.106 (0.004)	0.757

P-values given for adjusted group comparisons after correcting for age, gender and cross-sectional area.
a.u. = arbitrary unit.

significant association was seen between lower spinal tNAA concentrations and increased global and spinal-cord specific disability measures (as reflected by higher Expanded Disability Status Scale, Modified Ashworth Scale, Vibration Perception Threshold and postural sway, respectively) (Tables 4 and 5). Lower spinal Glx and higher myo-inositol were both also independently associated with increased postural instability (Table 5). When looking at

Table 4 Associations between whole cord measures (predictors) and clinical scores (response variables)

Clinical score	Spinal cord measure	Regression coefficient	95% Confidence interval	*P*-value
Expanded Disability Status Scale	tNAA	−0.41	−1.06, 0.34	$0.01 < P < 0.05$*
Summated Modified Ashworth Scale	tNAA	−3.78	−16.49, 2.16	$0.01 < P < 0.05$*
	P0*xy*	−283.72	−444.26, −123.19	0.002
	FWHM*xy*	191.30	86.36, 269.24	0.001
	ADC*xy*	63.64	18.89, 103.39	0.008
Mean grip	P0*xy*	435.96	−61.67, 933.59	0.081
Vibration Perception Threshold	tNAA	−4.37	−8.08, −0.66	0.021
	P0*xy*	−344.27	−512.61, −175.93	0.001
	FWHM*xy*	226.49	115.73, 337.26	0.001
	ADC*xy*	88.06	49.02, 127.10	<0.001

Unstandardized regression coefficients for imaging measures are reported with 95% confidence intervals and *P*-values. The regression models were adjusted for age, gender and mean cord area. *Bootstrap *P*-values.

the relationship between QSI measures and disability, increased QSI-derived perpendicular diffusivity was associated with higher spasticity (Modified Ashworth Scale), higher Vibration Perception Threshold, and increased postural instability (Tables 4 and 5).

Associations between column-specific q-space imaging indices and clinical disability

Following adjustment for age, gender, cross-sectional area, brain T_2 lesion volume, grey matter fractional volume and white matter fractional volume, increased perpendicular diffusivity within the major spinal columns was associated with increased disability. In particular, increased spasticity was independently associated with perpendicular diffusivity in all the columns (in particular, lower P0*xy* in the anterior, lateral and posterior columns, increased FWHM*xy* in the anterior and lateral columns, and increased ADC*xy* in the lateral columns). Reduced vibration sensation was independently associated with increased perpendicular diffusivity (reduced P0*xy* and increased FWHM*xy* and ADC*xy*) in the anterior, lateral and posterior columns. Instability in the roll plane was independently associated with increased perpendicular diffusivity (reduced P0*xy*) in the posterior column, while instability in the pitch plane was independently associated with increased perpendicular diffusivity (increased ADC*xy*) in the anterior column. A summary of associations is presented in Table 6.

Discussion

In this study, we have demonstrated lower concentrations of tNAA and Glx in the upper cervical cord of patients with early PPMS compared to control subjects, which suggest neuronal loss and/or metabolic dysfunction, and changes in the glutamatergic pathway. The increased QSI-derived perpendicular diffusivity (increased FWHM*xy* and decreased P0*xy*) in patients compared with controls further confirms the occurrence of reduced neuronal integrity, possibly with demyelination. Significant associations between spinal cord tNAA, Glx and QSI-derived perpendicular diffusivity and newer measures of clinical disability, such as postural stability and Vibration Perception Threshold, suggest that these imaging measures reflect abnormalities that contribute to clinical impairment. Thus, the evidence for early neurodegeneration in the spinal cord, in the absence of extensive spinal cord atrophy, and its link with clinical impairment, provide insights into the pathological events that occur in PPMS and indicate that this should become a target for therapeutic intervention.

Differences in metabolite concentrations and q-space imaging measures between patients and controls

The lower tNAA concentrations in the spinal cord of PPMS patients, when compared with healthy controls, are consistent with metabolite abnormalities in the brain, where tNAA is lower in cortical grey matter and normal-appearing white matter in early PPMS compared with controls (Sastre-Garriga *et al.*, 2005). In addition, our findings are qualitatively similar to those seen in acute (Ciccarelli *et al.*, 2007; Henning *et al.*, 2008; Ciccarelli *et al.*, 2010) and chronic (Marliani *et al.*, 2010; Ciccarelli *et al.*, 2013) spinal cord lesions in relapsing-remitting multiple sclerosis. The majority of patients with early PPMS included in the present study ($n = 12$) had a lesion (or part of a lesion) within the spectroscopic voxel and in these patients, spinal tNAA concentrations were lower than patients without a lesion. There were too few subjects in the study to detect a statistically significant difference in tNAA concentrations between patients with and without spinal lesions within the spectroscopic voxel: we estimated that the sample size required to detect a difference between those two groups with 80% power (alpha 0.05) using the spectroscopy protocol described in this study would be 168 subjects per group; this finding suggests that tNAA

Table 5 Associations between whole cord imaging measures and truncal stability

	Sway coefficient (95% CI; *P*-value)	Pitch coefficient (95% CI; *P*-value)	Roll coefficient (95% CI; *P*-value)	Romberg quotient coefficient (95% CI; *P*-value)
tNAA	***P* < 0.001**	***P* < 0.0001**	***P* = 0.005**	***P* = 0.003**
	4EO: −0.057 (−0.188, 0.074; *P* = 0.393)	4EO: −0.036 (−0.144, 0.073; *P* = 0.517)	4EO: −0.039 (−0.111, 0.033; *P* = 0.286)	4 cm: −0.112 (−0.191, −0.033; *P* = 0.006)
	4EC: −0.192 (−0.416, 0.033; *P* = 0.094)	4EC: −0.137 (−0.277, 0.003; *P* = 0.056)	4EC: −0.103 (−0.256, 0.049; *P* = 0.184)	32 cm: −0.191 (−0.123, 0.085; *P* = 0.718)
	32EO: −0.072 (−0.118, −0.022; *P* = 0.004)	32EO: −0.047 (−0.099, 0.006; *P* = 0.082)	32EO: −0.044 (−0.069, −0.018; *P* = 0.001)	
	32EC: −0.086 (−0.221, 0.048; *P* = 0.208)	32EC: −0.063 (−0.192, 0.066; *P* = 0.338)	32EC: −0.046 (−0.083, −0.009; *P* = 0.014)	
Glx	***P* = 0.017**	***P* < 0.001**	***P* = 0.012**	***P* < 0.0001**
	4EO: −0.171 (−0.301, −0.042; *P* = 0.010)	4EO: −0.110 (−0.227, 0.007; *P* = 0.065)	4EO: −0.108 (−0.171, −0.046; *P* = 0.001)	4 cm: −0.134 (−0.236, −0.032; *P* = 0.010)
	4EC: −0.320 (−0.564, −0.076; *P* = 0.010)	4EC: −0.204 (−0.360, −0.049; *P* = 0.010)	4EC: −0.207 (−0.367, −0.046; *P* = 0.012)	32 cm: −0.140 (0.232, −0.048; *P* = 0.003)
	32EO: −0.057 (−0.127, 0.014; *P* = 0.114)	32EO: −0.033 (−0.103, 0.038; *P* = 0.366)	32EO: −0.039 (−0.076, −0.002; *P* = 0.039)	
	32EC: −0.163 (−0.310, −0.015; *P* = 0.031)	32EC: −0.134 (−0.279, 0.010; *P* = 0.069)	32EC: −0.062 (−0.104, 0.020; *P* = 0.004)	
Ins	***P* < 0.0001**	***P* = 0.014**	***P* = 0.440**	***P* = 0.046**
	4EO: 0.062 (−0.061, 0.185; *P* = 0.324)	4EO: 0.068 (−0.324, 0.170; *P* = 0.184)		4 cm: 0.031 (−0.052, 0.113; *P* = 0.467)
	4EC: 0.100 (−0.102, 0.303; *P* = 0.332)	4EC: 0.062 (−0.078, 0.201; *P* = 0.388)		32 cm: 0.086 (−0.019, 0.153; *P* = 0.012)
	32EO: 0.019 (−0.065, 0.103; *P* = 0.660)	32EO: 0.026 (−0.045, 0.097; *P* = 0.477)		
	32EC: 0.090 (−0.010, 0.191; *P* = 0.078)	32EC: 0.093 (0.004, 0.183; *P* = 0.040)		
tCho	***P* = 0.545**	***P* = 0.144**	***P* = 0.979**	***P* = 0.113**
tCr	***P* = 0.306**	***P* = 0.237**	***P* = 0.821**	***P* = 0.363**
ADC*xy*		4EC: 2.48 (0.44, 4.51; *P* = 0.017)	32EO: 0.93 (0.34, 1.52; *P* = 0.002)	4 cm: 1.41 (0.24, 2.59; *P* = 0.023)
			32EC: 1.24 (0.28, 2.21; *P* = 0.011)	
FWHM*xy*		4EC: 5.57 (0.02, 11.12; *P* = 0.049)	32EO: 2.25 (0.56, 3.94; *P* = 0.009)	
P0*xy*			32EO: −3.80 (−6.14, −1.46; *P* = 0.001)	
			32EC: −5.01 (−8.84, −1.18; *P* = 0.010)	

A multivariate analysis was used to assess associations between metabolite predictors and the multiple stability scores as response variables. *P*-values <0.05 for the joint test of the metabolite predictor are shown in bold. Metabolite regression coefficients, 95% confidence intervals and *P*-values are shown for the individual stability variables, and these are only shown where the joint test was significant. The regression models adjusted for age, gender and mean cord area.
CI = confidence interval; tCr = creatine + phosphocreatine; Ins = myo-inositol; tCho = choline containing compounds; 4EC = stance width of 4 cm, eyes closed; 4EO = stance width of 4 cm, eyes open; 32EC = stance width of 32 cm, eyes closed; 32EO = stance width of 32 cm, eyes open.

Table 6 Associations between column-specific diffusion indices (predictors) and clinical scores (response variable)

Clinical score	Region of interest	Diffusion measure	Regression coefficient	95% Confidence interval	*P*-value
Summated Modified Ashworth Scale	Lateral column	P0*xy*	−205.16	−322.34, −87.97	0.002
		FWHM*xy*	171.80	91.34, 252.27	<0.001
		ADC*xy*	50.66	16.50, 84.83	0.006
	Anterior column	P0*xy*	−185.96	−316.30, −55.62	0.008
		FWHM*xy*	157.38	64.03, 250.72	0.002
	Posterior column	P0*xy*	−136.56	−267.09, −6.03	0.04
Vibration	Lateral column	P0*xy*	−268.54	−421.03, −116.05	0.002
		FWHM*xy*	223.44	125.91, 320.90	<0.001
		ADC*xy*	67.20	28.07, 106.33	0.002
	Anterior column	P0*xy*	−239.01	−384.52, −93.50	0.003
		FWHM*xy*	200.74	106.07,295.41	0.001
		ADC*xy*	40.73	7.82, 73.64	0.02
	Posterior column	P0*xy*	−219.76	−353.71, −85.80	0.003
		FWHM*xy*	101.77	32.47, 171.08	0.007
		ADC*xy*	46.29	22.24, 70.34	0.001
32EO Sway	Anterior column	ADC*xy*	0.81	0.12, 1.50	0.021
32EO Roll	Posterior column	P0*xy*	−2.16	−4.07, −0.26	0.026
32EO Pitch	Anterior column	ADC*xy*	0.69	0.15, 1.23	0.013
32EC Roll	Posterior column	P0*xy*	−3.85	−6.58, −1.12	0.006
32EC Pitch	Anterior column	ADC*xy*	1.04	0.12, 1.94	0.026
4EO Pitch	Anterior column	ADC*xy*	1.02	0.13, 1.91	0.025
4EC Pitch	Anterior column	ADC*xy*	1.54	0.47, 2.63	0.005
4 cm Romberg	Lateral column	ADC*xy*	1.18	0.20, 2.16	0.023

Unstandardized regression coefficients for imaging measures are reported with 95% confidence intervals and *P*-values. The regression models were adjusted for age, gender and mean cord area. 4EC = stance width of 4 cm, eyes closed; 4EO = stance width of 4 cm, eyes open; 32EC = stance width of 32 cm, eyes closed; 32EO = stance width of 32 cm, eyes open.

concentration is lowest in lesional tissue of the spinal cord, but may be reduced, although less extensively, in the normal-appearing white matter when compared with healthy tissue, which is similar to what has previously been demonstrated in the brain (Caramanos *et al.*, 2005).

Glx, which represents the sum of glutamate and its precursor glutamine, was also significantly lower in patients than controls. These changes were most significant in patients with spinal cord lesions within the spectroscopic voxel and likely reflect changes in the spinal glutamatergic pathway. Glutamate makes up the majority of the Glx signal (Baker *et al.*, 2008), and is predominantly found in the synaptic terminals, with relatively little present in the extracellular compartment and glial cells (Kaiser *et al.*, 2005; Muhlert *et al.*, 2014). It is therefore possible that lower spinal Glx could—in part—be explained by neuro-axonal degeneration. In the brains of patients with early PPMS, Glx is reduced in the cortical grey matter, but not the normal-appearing white matter (Sastre-Garriga *et al.*, 2005). Similarly, in patients with clinically stable relapsing-remitting multiple sclerosis, Glu and Glx are both reduced in grey matter regions (Muhlert *et al.*, 2014). Together these results would suggest that the reductions in Glx reflect reduced synaptic density in the grey matter secondary to neuronal loss. We found that Glx did not correlate well with tNAA, which suggests that impairment of glutamatergic metabolism as well as neuroaxonal loss may occur in early PPMS, and these metabolites reflect different aspects of the underlying tissue changes.

Using QSI we measured diffusivity, parallel and perpendicular to the long axis of the spinal cord and found significantly higher perpendicular diffusivity in patients compared with controls. The changes in the displacement probability density function shape (Fig. 2) in our patient group are likely to reflect a breakdown in myelin and axonal membranes, which both act as microstructural barriers to perpendicular diffusion (Beaulieu, 2002) and correspond to what would be expected based on findings from murine and canine models of dysmyelination and axonal loss (Biton *et al.*, 2006; Farrell *et al.*, 2010; Wu *et al.*, 2011; Anaby *et al.*, 2013), as well as to what has previously been reported in patients with relapse-onset multiple sclerosis (Assaf *et al.*, 2002; Farrell *et al.*, 2008). The differences in QSI measures between patients and controls are also in agreement with the tNAA and Glx changes detected and provide corroborating evidence for early neurodegeneration in the cervical cord. Importantly, in patients with normal-appearing spinal tissue within the diffusion imaging volume, FWHM*xy* and P0*xy* remained significantly different to controls, whereas ADC*xy* did not, suggesting that QSI indices are more sensitive to microstructural injury than conventional ADC measures.

In addition to the differences in tNAA, Glx and QSI-derived perpendicular diffusivity between groups, we found that patients had higher spinal myo-inositol levels than controls but this finding did not reach statistical significance. We calculated that for myo-inositol, to have 80% power to detect a patient versus control difference of the size observed

(which is about two-thirds of a standard deviation) at 5% significance, 40 subjects per group would be necessary. Patients with a spinal cord lesion within the spectroscopic voxel did have significantly elevated myo-inositol concentrations, which is likely to reflect astrocytic proliferation and activation (or gliosis) in spinal cord lesions in early PPMS. Previous studies have suggested that gliosis is an early pathological process in multiple sclerosis, and gliosis may be an important mechanism of disease progression (Ciccarelli *et al.*, 2014). Our results suggest this process is more active in lesional than non-lesional tissue.

With regard to total choline, which is a marker of inflammation and membrane turnover (Henning *et al.*, 2008; Marliani *et al.*, 2010), since the observed differences between groups is $<15\%$ of the standard deviation, it would take hundreds of subjects per arm to detect such a small difference, suggesting that this metabolite is unlikely to be useful for distinguishing patients from healthy controls in future studies.

In our study, spinal cross-sectional area, a measure of tissue loss, which is often used as an imaging surrogate of axonal loss and has started to be used in multiple sclerosis clinical trials (Kearney *et al.*, 2013), was not significantly different between patients and controls despite cross-sectional area measurements being performed on a sequence with high in-plane resolution. Earlier studies with larger sample sizes (Bieniek *et al.*, 2006) and those which included patients with longer disease duration (Losseff *et al.*, 1996), demonstrated significant cord atrophy in PPMS. Based on cross-sectional area measures from our cohort of patients and controls, we estimate that the sample size required to detect significant differences in cross-sectional area in early PPMS, using the method described in this study with 80% power (alpha = 0.05), is 68 subjects per group. This would suggest that much smaller sample sizes are required to detect group differences early in the disease course with newer quantitative MRI measures that reflect neurodegenerative processes other than atrophy alone. We cannot exclude that alternative image segmentation methods, such as the edge detection and partial volume correction method proposed by Tench and colleagues (2005) may have enabled detection of significant cord atrophy in this patient group and this merits further study in future. To validate these new measures for clinical trials, it is important to test whether these quantitative MRI measures and metabolite concentrations are sensitive to changes occurring over time and predict clinical outcome at follow-up.

Association between spinal cord metabolites and diffusion indices

The modifications to gradients and pulse lengths necessary to perform QSI on clinical scanners have the effect of exaggerating the contribution of slow diffusing water to QSI metrics (Assaf *et al.*, 2002), consequently, diffusion of intra-axonal water is highly represented (Assaf *et al.*, 2000, 2005; Assaf and Cohen, 2000) and it has therefore been suggested that QSI metrics make useful markers of axonal integrity. Interestingly, in our study, spinal tNAA concentration, which reflects axonal integrity, correlated more strongly with QSI-derived indices of perpendicular diffusivity than ADC, suggesting that these indices are more indicative of axonal integrity.

Associations between whole cord imaging measurements and clinical disability

Using new clinical scales, which reflect disability in functions mediated by spinal cord pathways, we have extended previous findings of significant associations between tNAA and neurological disability, as measured by the Expanded Disability Status Scale, in the spinal cord of patients with relapsing-remitting multiple sclerosis (Blamire *et al.*, 2007; Ciccarelli *et al.*, 2007), by demonstrating that significant associations exist in patients with early PPMS and that Glx levels are associated with postural stability.

We found that, in patients, higher myo-inositol concentrations were associated with poor postural stability, suggesting that spinal cord gliosis may be a process of clinical importance in early PPMS. This is in agreement with spinal cord MRS studies in relapsing-remitting multiple sclerosis, which have shown an increased myo-inositol concentration in patients than controls (Marliani *et al.*, 2010) and a relationship between higher myo-inositol and higher Expanded Disability Status Scale scores (Ciccarelli *et al.*, 2007).

In agreement with the MRS results, we found that increased whole cord QSI-derived perpendicular diffusivity, which reflects increased movement of water in the direction perpendicular to the main axis of the cord, as a consequence of reduced neuronal integrity and/or demyelination, is independently associated with increased spasticity, Vibration Perception Thresholds and postural instability. Our findings extend on those from an earlier pilot study which found a significant increase in QSI-derived perpendicular diffusivity within spinal cord lesions in patients with relapse-onset multiple sclerosis compared to healthy controls (Farrell *et al.*, 2008), and suggest that whole cord QSI reflects clinically meaningful pathological changes in the spinal cord.

Associations between column-specific diffusion indices and disability

We found several significant associations that were expected based on *a priori* knowledge of the neurological function of tracts running in specific spinal cord columns. Specifically, increased QSI-derived perpendicular diffusivity within the anterior and lateral columns, where the

corticospinal tracts are located, independently predicted spasticity. Instability in the roll plane and diminished vibration sense were predicted by increased perpendicular diffusivity in the posterior columns, where afferent sensory tracts conveying vibration sense and proprioception run. It is interesting that this effect emerges with the feet wider apart, when the body is normally more stable. It has previously been suggested that the increased stability with increasing stance width, in part, arises from hip proprioceptors being increasingly able to signal lateral sway, because of the mechanical linkage between hips and ankles (Day *et al.*, 1993), which may be degraded where there is posterior column pathology. When we examined the association between the imaging measures and postural stability, we found that higher ADC*xy* in the anterior column was associated with increased instability in the pitch plane, which implies that pitch plane abnormalities are predominantly linked to pathology of the tracts running in the anterior columns that mediate motor organization or coordination. The coordination of joints is probably more demanding in the sagittal (pitch) plane as there are more degrees of freedom due to independent action of leg joints. In contrast, in the frontal (roll) plane, the knees cannot contribute much to instability, while the ankle and hips are no longer independent (Day *et al.*, 1993).

For associations between imaging and clinical measures, we did not adjust for multiple comparisons as we were investigating a number of different hypotheses, and in such contexts, correction can be inappropriate (Rothman, 1990; Perneger, 1998); nevertheless, as always there is a danger of spurious significant results, and *P*-values close to 0.05 should be interpreted with caution and regarded as hypothesis-generating, to be examined in future studies.

Limitations and future directions

Although we have used state-of-the-art spinal cord sequences, there are a number of limitations of the current study that future work could try to address. Using a clinical scanner, our MRS protocol reliably quantified Glx in the spinal cord for the first time in a group of patients with multiple sclerosis. Strategies for separating glutamine and glutamate at 3 T, such as echo time averaged PRESS, have been developed and used in the brain (Hurd *et al.*, 2004; Hancu, 2009), but they may not be feasible in the spinal cord, using a 3 T scanner because much larger voxel sizes would be needed. Future technical developments may make it possible to directly measure glutamate with no glutamine overlap in the spinal cord, which would allow a more specific evaluation of the role of glutamate in multiple sclerosis pathophysiology in the spinal cord.

In addition, the smaller gradients and longer gradient pulses needed to perform QSI on a clinical scanner have the effect of narrowing the displacement probability density function produced by q-space analysis, possibly leading to an under-estimate of the FWHM. It has been proposed that these should be considered as apparent values (Assaf *et al.*, 2005; Farrell *et al.*, 2008). Therefore direct comparison with previously published studies should be made with care, and only after taking into account differences in gradient settings.

It was beyond the scope of the current study to establish whether the QSI indices used in this study are more sensitive to spinal microstructural changes than the more established DTI-derived indices, such as fractional anisotropy, radial and axial diffusivity. An attempt to address this question has been made in the past. Assaf *et al.* (2002) examined 13 patients with multiple sclerosis using diffusion tensor imaging and QSI and demonstrated greater sensitivity of q-space metrics at detecting abnormalities in the normal-appearing white matter and lesional brain tissue compared with fractional anisotropy. This finding was reproduced in a later study from the same group (Assaf *et al.*, 2005), when they also showed that q-space displacement values correlated strongly to NAA/creatine ratios, suggesting that they are highly specific for axonal loss.

A future longitudinal extension of the current study will investigate whether QSI and MRS measures are predictive of disability and cord atrophy at 1 year and 3 years. We will also examine whether the predictive accuracy can be improved by combing metabolic and structural metrics into a parametric model. Application of these new imaging techniques to patients with other multiple sclerosis subtypes is also required. This information may help to stratify patients for treatments and clinical trials on the basis of their spinal cord pathology and predicted clinical course. Further work is needed to establish the relationship between QSI-derived indices from the lateral columns and lateralized disability and to assess how closely longitudinal changes in imaging measures reflect clinical change in order to validate the use of these advanced spinal cord imaging protocols to provide potential imaging biomarkers for future clinical trials of neuroprotective agents.

Funding

The NMR Research Unit is supported by the UK MS Society. This study has been supported by the UK MS Society (Award Ref No: 984). T.S. is supported by the EPSRC (grant reference EP/I027084/1). This work was undertaken at UCLH/UCL who received a proportion of funding from the Department of Health's NIHR Biomedical Research Centres funding scheme.

Supplementary material

Supplementary material is available at *Brain* online.

References

Anaby D, Duncan ID, Smith CM, Cohen Y. q-Space diffusion MRI (QSI) of the disease progression in the spinal cords of the Long Evans shaker: diffusion time and apparent anisotropy. NMR Biomed 2013; 26: 1879–86.

Assaf Y, Ben-Bashat D, Chapman J, Peled S, Biton IE, Kafri M, et al. High b-value q-space analyzed diffusion-weighted MRI: application to multiple sclerosis. Magn Reson Med 2002; 47: 115–26.

Assaf Y, Chapman J, Ben-Bashat D, Hendler T, Segev Y, Korczyn AD, et al. White matter changes in multiple sclerosis: correlation of q-space diffusion MRI and 1H MRS. Magn Reson Imaging 2005; 23: 703–10.

Assaf Y, Cohen Y. Assignment of the water slow-diffusing component in the central nervous system using q-space diffusion MRS: implications for fiber tract imaging. Magn Reson Med 2005; 43: 191–99.

Assaf Y, Mayk A, Cohen Y. Displacement imaging of spinal cord using q-space diffusion-weighted MRI. Magn Reson Med 2000; 44: 713–22.

Baker EH, Basso G, Barker PB, Smith MA, Bonekamp D, Horska A. Regional apparent metabolite concentrations in young adult brain measured by (1)H MR spectroscopy at 3 Tesla. J Magn Reson Imaging 2008; 27: 489–99.

Beaulieu C. The basis of anisotropic water diffusion in the nervous system - a technical review. NMR Biomed 2002; 15: 435–55.

Bieniek M, Altmann DR, Davies GR, Ingle GT, Rashid W, Sastre-Garriga J, et al. Cord atrophy separates early primary progressive and relapsing remitting multiple sclerosis. J Neurol Neurosurg Psychiatry 2006; 77: 1036–39.

Biton IE, Duncan ID, Cohen Y. High b-value q-space diffusion MRI in myelin-deficient rat spinal cords. Magn Reson Imaging 2006; 24: 161–66.

Bjartmar C, Kidd G, Mork S, Rudick R, Trapp BD. Neurological disability correlates with spinal cord axonal loss and reduced N-acetyl aspartate in chronic multiple sclerosis patients. Ann Neurol 2000; 48: 893–901.

Blamire AM, Cader S, Lee M, Palace J, Matthews PM. Axonal damage in the spinal cord of multiple sclerosis patients detected by magnetic resonance spectroscopy. Magn Reson Med 2007; 58: 880–5.

Bodini B, Cercignani M, Toosy A, Stefano ND, Miller DH, Thompson AJ, et al. A novel approach with "skeletonised MTR" measures tract-specific microstructural changes in early primary-progressive MS. Hum Brain Mapp 2013; 35: 723–33.

Bohannon RW, Smith MB. Interrater reliability of a modified Ashworth scale of muscle spasticity. Phys Ther 1987; 67: 206–7.

Brand A, Richter-Landsberg C, Leibfritz D. Multinuclear NMR studies on the energy metabolism of glial and neuronal cells. Dev Neurosci 1993; 15: 289–98.

Bunn LM, Marsden JF, Giunti P, Day BL. Stance instability in spinocerebellar ataxia type 6. Mov Disord 2013; 28: 510–16.

Callaghan PT, Eccles CD, Xia Y. NMR microscopy of dynamic displacements: k-space and q-space imaging. J Phy E Sci Instrum 1988; 21: 820.

Caramanos Z, Narayanan S, Arnold DL. 1H-MRS quantification of tNA and tCR in patients with multiple sclerosis: a meta-analytic review. Brain 2005; 128: 2483–506.

Chard DT, Jackson JS, Miller DH, Wheeler-Kingshott CA. Reducing the impact of white matter lesions on automated measures of brain gray and white matter volumes. J Magn Reson Imaging 2010; 32: 223–8.

Ciccarelli O, Altmann DR, McLean MA, Wheeler-Kingshott CA, Wimpey K, Miller DH, et al. Spinal cord repair in MS: does mitochondrial metabolism play a role? Neurology 2010; 74: 721–7.

Ciccarelli O, Barkhof F, Bodini B, De Stefano N, Golay X, Nicolay K, et al. Pathogenesis of multiple sclerosis: insights from molecular and metabolic imaging. Lancet Neurol 2014; 13: 807–22.

Ciccarelli O, Thomas D, De Vita E, Wheeler-Kingshott C, Kachramanoglou C, Kapoor R, et al. Low myo-inositol indicating astrocytic damage in a case series of NMO. Ann Neurol 2013; 74: 301–5.

Ciccarelli O, Wheeler-Kingshott CA, McLean MA, Cercignani M, Wimpey K, Miller DH, et al. Spinal cord spectroscopy and diffusion-based tractography to assess acute disability in multiple sclerosis. Brain 2007; 130: 2220–31.

Confavreux C, Vukusic S, Moreau T, Adeleine P. Relapses and progression of disability in multiple sclerosis. N Engl J Med 2000; 343: 1430–8.

Cottrell DA, Kremenchutzky M, Rice GP, Koopman WJ, Hader W, Baskerville J, et al. The natural history of multiple sclerosis: a geographically based study. 5. The clinical features and natural history of primary progressive multiple sclerosis. Brain 2000; 122: 625–39.

Cutter GR, Baier ML, Rudick RA, Cookfair DL, Fischer JS, Petkau J, et al. Development of a multiple sclerosis functional composite as a clinical trial outcome measure. Brain 1999; 122: 871–82.

Day BL, Steiger MJ, Thompson PD, Marsden CD. Effect of vision and stance width on human body motion when standing: implications for afferent control of lateral sway. J Physiol 1993; 469: 479–99.

Edden RA, Bonekamp D, Smith MA, Dubey P. Barker PB Proton MR spectroscopic imaging of the medulla and cervical spinal cord. J Magn Reson Imaging 2007; 26: 1101–5.

Farrell JA, Smith SA, Gordon-Lipkin EM, Reich DS, Calabresi PA, van Zijl PC. High b-value q-space diffusion-weighted MRI of the human cervical spinal cord *in vivo*: feasibility and application to multiple sclerosis. Magn Reson Med 2008; 59: 1079–89.

Farrell JA, Zhang J, Jones MV, Deboy CA, Hoffman PN, Landman BA, et al. q-space and conventional diffusion imaging of axon and myelin damage in the rat spinal cord after axotomy. Magn Reson Med 2010; 63: 1323–35.

Fischer JS, Rudick RA, Cutter GR, Reingold SC. The Multiple Sclerosis Functional Composite Measure (MSFC): an integrated approach to MS clinical outcome assessment. National MS Society Clinical Outcomes Assessment Task Force. Mult Scler 1999; 5: 244–250.

Fox RJ, Thompson A, Baker D, Baneke P, Brown D, Browne P, et al. Setting a research agenda for progressive multiple sclerosis: the International Collaborative on Progressive MS. Mult Scler 2012; 18: 1534–40.

Gasparovic C, Song T, Devier D, Bockholt HJ, Caprihan A, Mullins PG, et al. Use of tissue water as a concentration reference for proton spectroscopic imaging. Magn Reson Med 2006; 55: 1219–26.

Goodkin DE, Hertsgaard D, Seminary J. Upper extremity function in multiple sclerosis: improving assessment sensitivity with box-and-block and nine-hole peg tests. Arch Phys Med Rehabil 1988; 69: 850–4.

Hancu I. Optimized glutamate detection at 3T. J Magn Reson Imaging 2009; 30: 1155–62.

Henning A, Schar M, Kollias SS, Boesiger P, Dydak U. Quantitative magnetic resonance spectroscopy in the entire human cervical spinal cord and beyond at 3T. Magn Reson Med 2008; 59: 1250–8.

Hobart JC, Riazi A, Lamping DL, Fitzpatrick R. Thompson AJ Measuring the impact of MS on walking ability: the 12-Item MS Walking Scale (MSWS-12). Neurology 2003; 60: 31–6.

Horsfield MA, Sala S, Neema M, Absinta M, Bakshi A, Sormani MP, et al. Rapid semi-automatic segmentation of the spinal cord from magnetic resonance images: application in multiple sclerosis. Neuroimage 2010; 50: 446–55.

Hurd R, Sailasuta N, Srinivasan R, Vigneron DB, Pelletier D, Nelson SJ. Measurement of brain glutamate using TE-averaged PRESS at 3T. Magn Reson Med 2004; 51: 435–40.

Kaiser LG, Schuff N, Cashdollar N, Weiner MW. Age-related glutamate and glutamine concentration changes in normal human brain: 1H MR spectroscopy study at 4 T. Neurobiol Aging 2005; 26: 665–72.

Kearney H, Yiannakas MC, Abdel-Aziz K, Wheeler-Kingshott CA, Altmann DR, Ciccarelli O, Miller DH. Improved MRI quantification of spinal cord atrophy in multiple sclerosis. J Magn Reson Imaging 2013; 39: 617–23.

Kearney H, Yiannakas MC, Samson RS, Wheeler-Kingshott CA, Ciccarelli O, Miller DH. Investigation of magnetization transfer ratio-derived pial and subpial abnormalities in the multiple sclerosis spinal cord. Brain 2014; 137: 2456–68.

Khaleeli Z, Ciccarelli O, Manfredonia F, Barkhof F, Brochet B, Cercignani M, et al. Predicting progression in primary progressive multiple sclerosis: a 10-year multicenter study. Ann Neurol 2008; 63: 790–3.

Khaleeli Z, Sastre-Garriga J, Ciccarelli O, Miller DH, Thompson AJ. Magnetisation transfer ratio in the normal appearing white matter predicts progression of disability over 1 year in early primary progressive multiple sclerosis. J Neurol Neurosurg Psychiatry 2007; 78: 1076–82.

Kurtzke JF. Rating neurologic impairment in multiple sclerosis: an expanded disability status scale (EDSS). Neurology 1983; 33: 1444–52.

Losseff NA, Webb SL, O'Riordan JI, Page R, Wang L, Barker GJ, et al. Spinal cord atrophy and disability in multiple sclerosis. A new reproducible and sensitive MRI method with potential to monitor disease progression. Brain 1996; 119: 701–8.

Marliani AF, Clementi V, Albini-Riccioli L, Agati R, Leonardi M. Quantitative proton magnetic resonance spectroscopy of the human cervical spinal cord at 3 tesla. Magn Reson Med 2007; 57: 160–3.

Marliani AF, Clementi V, Albini Riccioli L, Agati R, Carpenzano M, Salvi F, Leonardi M. Quantitative cervical spinal cord 3T proton MR spectroscopy in multiple sclerosis. AJNR Am J Neuroradiol 2010; 31: 180–4.

Moffett JR, Ross B, Arun P, Madhavarao CN, Namboodiri AM. N-Acetylaspartate in the CNS: from neurodiagnostics to neurobiology. Prog Neurobiol 2007; 81: 89–131.

Muhlert N, Atzori M, De Vita E, Thomas DL, Samson RS, Wheeler-Kingshott CA, et al. Memory in multiple sclerosis is linked to glutamate concentration in grey matter regions. J Neurol Neurosurg Psychiatry 2014; 85: 833–9.

Oh J, Saidha S, Chen M, Smith SA, Prince J, Jones C, et al. Spinal cord quantitative MRI discriminates between disability levels in multiple sclerosis. Neurology 2013; 80: 540–7.

Ourselin S, Roche A, Prima S, Ayache N. Block Matching: a general framework to improve robustness of rigid registration of medical images. In: Delp S, DiGoia A, Jaramaz B, editors. . Medical Image Computing and Computer-Assisted Intervention – MICCAI 2000. Vol. 1935. Berlin Heidelberg: Springer; 2000. p. 557–66.

Perneger TV. What's wrong with Bonferroni adjustments. BMJ 1998; 316: 1236–8.

Polman CH, Reingold SC, Edan G, Filippi M, Hartung HP, Kappos L, et al. Diagnostic criteria for multiple sclerosis: 2005 revisions to the "McDonald Criteria". Ann Neurol 2005; 58: 840–6.

Provencher SW. Estimation of metabolite concentrations from localized *in vivo* proton NMR spectra. Magn Reson Med 1993; 30: 672–9.

Provencher SW. LCModel & LCMgui User's Manual. Vol. 2014. 2014. Available from http://s-provencher.com/pub/LCModel/manual/manual.pdf..

Ramio-Torrenta L, Sastre-Garriga J, Ingle GT, Davies GR, Ameen V, Miller DH, et al. Abnormalities in normal appearing tissues in early primary progressive multiple sclerosis and their relation to disability: a tissue specific magnetisation transfer study. J Neurol Neurosurg Psychiatry 2006; 77: 40–5.

Rothman KJ. No adjustments are needed for multiple comparisons. Epidemiology 1990; 1: 43–6.

Runmarker B, Andersen O. Prognostic factors in a multiple sclerosis incidence cohort with twenty-five years of follow-up. Brain 1993; 116: 117–34.

Sastre-Garriga J, Ingle GT, Chard DT, Ramio-Torrenta L, McLean MA, Miller DH, et al. Metabolite changes in normal-appearing gray and white matter are linked with disability in early primary progressive multiple sclerosis. Arch Neurol 2005; 62: 569–73.

Schneider T, Ciccarelli O, Kachramanoglou C, Thomas DL, Wheeler-Kingshott CAM. Reliability of tract-specific q-space imaging metrics in healthy spinal cord. Proc Intl Soc Mag Reson Med 2011; 66.

Smith SA, Levante TO, Meier BH, Ernst RR. Computer-simulations in magnetic-resonance - an object-oriented programming approach. J Magn Reson A 1994; 106: 75–105.

Solanky BS, Abdel-Aziz K, Yiannakas MC, Berry AM, Ciccarelli O, Wheeler-Kingshott CA. In vivo magnetic resonance spectroscopy detection of combined glutamate-glutamine in healthy upper cervical cord at 3 T. NMR Biomed 2013; 26: 357–66.

Stein J, Narendran K, McBean J, Krebs K, Hughes R. Electromyography-controlled exoskeletal upper-limb-powered orthosis for exercise training after stroke. Am J Phys Med Rehabil 2007; 86: 255–61.

Svens B, Lee H. Intra- and inter-instrument reliability of Grip-Strength Measurements: GripTrack™ and Jamar® hand dynamometers. Br J Hand Ther 2005; 10: 47–55.

Tench CR, Morgan PS, Constantinescu CS. Measurement of cervical spinal cord cross-sectional area by MRI using edge detection and partial volume correction. J Magn Reson Imaging 2005; 21: 197–203.

Thompson AJ, Montalban X, Barkhof F, Brochet B, Filippi M, Miller DH, et al. Diagnostic criteria for primary progressive multiple sclerosis: a position paper. Ann Neurol 2000; 47: 831–5.

Wansapura JP, Holland SK, Dunn RS, Ball WS. NMR relaxation times in the human brain at 3.0 tesla. J Magn Reson Imaging 1999; 9: 531–8.

Wheeler-Kingshott CA, Stroman PW, Schwab JM, Bacon M, Bosma R, Brooks J, et al. The current state-of-the-art of spinal cord imaging: applications. Neuroimage 2014; 84: 1082–93.

Wilm BJ, Svensson J, Henning A, Pruessmann KP, Boesiger P, Kollias SS. Reduced field-of-view MRI using outer volume suppression for spinal cord diffusion imaging. Magn Reson Med 2007; 57: 625–30.

Wu YC, Field AS, Duncan ID, Samsonov AA, Kondo Y, Tudorascu D, Alexander AL. High b-value and diffusion tensor imaging in a canine model of dysmyelination and brain maturation. Neuroimage 2011; 58: 829–37.

Yiannakas MC, Kearney H, Samson RS, Chard DT, Ciccarelli O, Miller DH, et al. Feasibility of grey matter and white matter segmentation of the upper cervical cord *in vivo*: a pilot study with application to magnetisation transfer measurements. Neuroimage 2012; 63: 1054–59.

Zackowski KM, Smith SA, Reich DS, Gordon-Lipkin E, Chodkowski BA, Sambandan DR, et al. Sensorimotor dysfunction in multiple sclerosis and column-specific magnetization transfer-imaging abnormalities in the spinal cord. Brain 2009; 132: 1200–9.